Turkish Journal of Electrical Engineering & Computer Sciences

http://journals.tubitak.gov.tr/elektrik/

Research Article

Turk J Elec Eng & Comp Sci
(2016) 24: 4027 – 4041

doi:10.3906/elk-1410-48

Vector control of a three-phase parallel connected two motor single inverter speed sensorless drive

Gunabalan RAMACHANDRAN[1,*], Subbiah VEERANA[2], Sanjeevikumar PADMANABAN[3]
[1]Department of EEE, VIT University, Chennai Campus, Tamil Nadu, India
[2]Department of EEE, PSG College of Technology, Coimbatore, Tamil Nadu, India
[3]Research and Development, Ohm Technologies, India

Received: 10.10.2014 • **Accepted/Published Online:** 03.07.2015 • **Final Version:** 20.06.2016

Abstract: This paper presents the performance characteristics of two induction motors of the same parameters and ratings connected in parallel and fed by a single inverter. A nature observer is employed to estimate the rotor speeds and rotor fluxes of both induction motors. It also estimates the load torques of both the motors by load torque adaptation. Under unbalanced load conditions, the speed difference between the two induction motors is reduced by considering the average and differential motor parameters and currents. Mean rotor flux is maintained constant by a rotor flux control scheme and the estimation of rotor angle is carried out by direct vector control technique. The prototype experimental setup is made for validating the proposed method and the experimental results are demonstrated for various running conditions. The natural observer algorithm for speed and torque estimation is executed by TMS320F2812 DSP controller.

Key words: Field oriented control, induction motor, natural observer, sensorless vector control, torque estimation

1. Introduction

Induction motors are preferred in most industries because of their simple structure, ruggedness, reliability, low cost, and less maintenance. For control purpose, encoders or tacho-generators sense the speed of the induction motor. In recent years, various speed and position sensorless control schemes have been developed for variable speed ac drives. The main reasons for the development of these sensorless drives are as follows: reduction of hardware complexity, increased mechanical robustness and overall ruggedness, higher reliability, decreased maintenance requirements, increased noise immunity, and elimination of sensor cables. This leads to the modern technology of speed sensorless vector control. Based on the information of line voltages and currents, speed can be estimated and its accuracy mostly meant for single inverter driven single induction motors. Multiple induction motors controlled by a single inverter run in parallel in electric traction drives to reduce the cost, size, and need for maintenance. If the machines have the same speed-torque characteristics then speeds are equal, and torque-sharing rates are equal in all operating conditions. Practically, there will be observable differences between the behaviors of machines and the speeds may not be identical because of slight differences in wheel diameters. The speed-torque characteristics for slightly far from identical machines are shown in Figure 1 (dark blue – motor 2, green line – motor 1), which causes different torque sharing at the same speed. By assuming that the wheel diameter of machine 1 is a bit larger than that of machine 2, then the torque sharing of machine 1 will be higher in motoring mode, but lower in braking mode where the corresponding characteristic is represented in Figure 1 (blue line). Both the mismatch in characteristics and unequal wheel diameter problems exist in

*Correspondence: gunabalanr@yahoo.co.in

real-time situations and the speed-torque behavior of both motors will differ and unbalance condition arises (red line – motor 1 and pink line – motor 2). If average currents flow through the stator windings and rotor fluxes are considered for unbalanced load conditions, the speeds of both motors deviate much from the command speed. To reduce the speed difference among the induction motors, average and differential currents were used to determine the reference currents [1,2] and the hardware results were presented only for step change in speed under no load conditions.

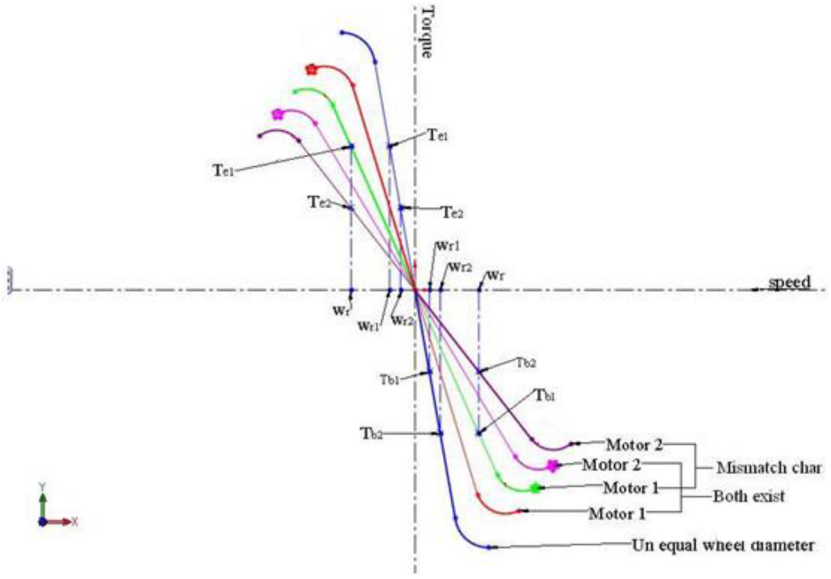

Figure 1. Speed-torque characteristics of parallel connected induction motor drives.

A parallel connected dual induction motor drive fed by a single inverter was discussed in [3,4], where simulation works were reported for unbalanced load conditions and experimental results were provided for step change in speed for no load conditions.

A low cost matrix converter with slip-frequency vector control was discussed in [5,6]. To minimize the speed difference between the induction motors for unbalanced load conditions, two degrees of freedom control is applied and only simulation results were provided. A novel control strategy based on weighted voltage vector was proposed [7] to relieve the thrust difference in each wheel with a parallel connected induction motor drive. Simulation results were presented for wheel radial difference, curve radius, and parameter difference. The effects of deviation of the wheel diameters on motor current, rotor speed, and torque for parallel operation was presented in [8]. Simulation results were provided for change in wheel diameter between front and rear wheels. To improve the control performance of dual speed-irrelevant motors for unbalanced load, weighted flux linkage vector control was used in [9]. The speed of the induction motors was controlled by PI-controller for one motor and P-controller for another motor. Simulation and hardware results were reported for different running conditions.

In the literature dealing with sensorless vector control of a parallel connected induction motor drive [1–4,10–14] an adaptive rotor flux observer was employed to estimate the speed and rotor fluxes of both the motors. The selection of gain matrix constant k is a tedious task in the adaptive rotor flux observer, where the typical value of k is taken as 0.5. It is mandatory to have correction factors to track the speed variations that result in estimation lags in the actual command signal. To overcome the above difficulties, a natural observer

[15] is proposed in this paper because of its simple structure to estimate the load torque of both the motors. A direct field oriented vector control scheme will be employed to calculate the flux angle and the average rotor flux derived from both induction motors will be kept constant by rotor flux feedback control [16,17]. Average and differential currents flowing through the stator and rotor fluxes will be used to calculate the reference currents. In the research papers dealing with parallel connected induction motor drives [1–4], the hardware results were presented for step change in speed under no load conditions, and in [5–8,10–14] only simulations results were presented. In this paper, experimental results are presented for balanced and unbalanced load conditions to prove the effectiveness of the proposed method. Simulation results are provided for step change in speed with constant load.

The paper is organized as follows: section 2 discusses the concepts of a natural observer. Parallel connected induction motor drives with necessary equations are presented in section 3. Simulation and experimental results are presented for various running conditions in section 4, and it is finally concluded in section 5.

2. Speed estimation using a natural observer

The structure and features of the natural observer are identical to the induction motor for the given supply voltage and load torque. The major difference between a natural observer and the conventional observer is that there is no direct external feedback and a faster convergence rate. As a result, the speed estimation follows the speed changes simultaneously. Figures 2(a) and 2(b) show the block diagram of the natural observer and the natural observer with load torque adaptation, respectively. Load torque adaptation is used to estimate the load torque from the active power error. A fourth order state space induction motor model in stator flux oriented reference frame is used to estimate the speed, where dq-axes stator currents and rotor fluxes are selected as state variables. A fifth order state space induction motor model is used in the literature [15]. The induction motor and the observer are represented in the stationary reference frame by the following state equations:

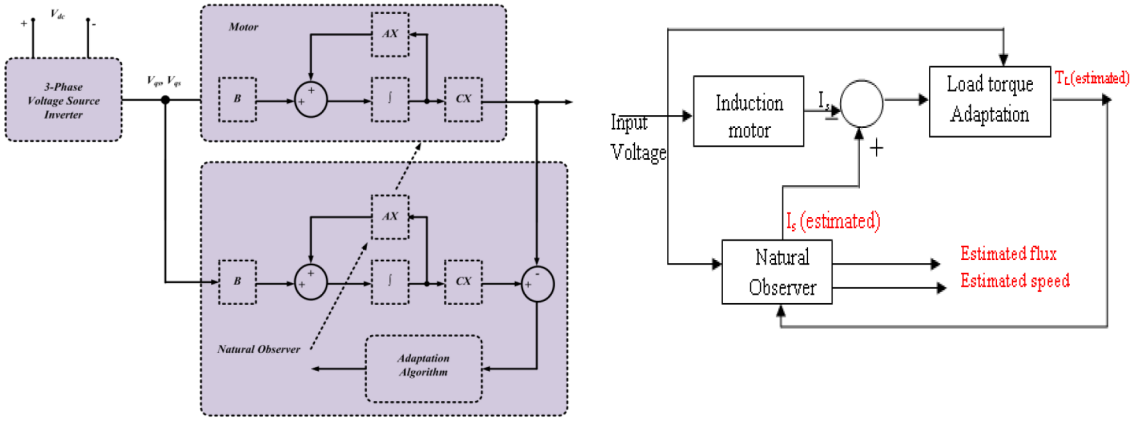

Figure 2. Block diagram of a natural observer.

$$\frac{dX}{dt} = AX + BV_s \tag{1}$$

$$Y = CX, \tag{2}$$

where

$$A=\begin{bmatrix} \frac{-1}{T_s} & 0 & \frac{L_m}{L_s' L_r \tau_r} & \frac{\omega_r L_m}{L_s' L_r} \\ 0 & \frac{-1}{T_s} & \frac{-\omega_r L_m}{L_s' L_r} & \frac{L_m}{L_s' L_r \tau_r} \\ \frac{L_m}{\tau_r} & 0 & \frac{-1}{\tau_r} & -\omega_r \\ 0 & \frac{L_m}{\tau_r} & \omega_r & \frac{-1}{\tau_r} \end{bmatrix}; B=\begin{bmatrix} \frac{1}{\sigma L_s} & 0 \\ 0 & \frac{1}{\sigma L_s} \\ 0 & 0 \\ 0 & 0 \end{bmatrix}; C=\begin{bmatrix} 1 & 0 & 0 & 0 \\ 0 & 1 & 0 & 0 \end{bmatrix}$$

$$\frac{1}{T_s}=\frac{R_s+R_r\left(\frac{L_m}{L_r}\right)\left(\frac{L_m}{L_r}\right)^2}{L_s'}; L_s^{'}=\sigma L_s.$$

$\sigma = 1-\frac{L_m^2}{L_s L_r}-$ Leakage coefficient.

$$X=\begin{bmatrix} i_{ds}^s & i_{qs}^s & \varphi_{dr}^s & \varphi_{qr}^s \end{bmatrix}^T; Y=\begin{bmatrix} i_{ds}^s & i_{qs}^s \end{bmatrix}=i_s; V_s=\begin{bmatrix} V_{ds}^s & V_{qs}^s \end{bmatrix}^T.$$

$$\frac{d\hat{X}}{dt}=\hat{A}\hat{X}+BV_s \tag{3}$$

$$\hat{Y}=C\hat{X} \tag{4}$$

The system described by Eqs. (3) and (4) is exactly the same form as the induction motor model without any external feedback. Load torque is estimated by the active power error as the correction term and is given by

$$\hat{T_L}=K_P e_P+K_I\int e_P dt, \tag{5}$$

where $e_P=V_{ds}^s\left(\hat{i}_{ds}^e-i_{ds}^e\right)+V_{qs}^s\left(\hat{i}_{qs}^e-i_{qs}^e\right)$ (6)

Estimation of rotor speed is acquired from estimated stator current, rotor flux, and the estimated load torque as:

$$\dot{\hat{\omega}_r}=\left(\frac{3}{2}\right)\left(\frac{n_p}{J}\right)\left(\frac{L_m}{L_r}\right)\left[\hat{\varphi}_{dr}^s\hat{i}_{qs}^s-\hat{\varphi}_{qr}^s\hat{i}_{ds}^s\right]-\frac{\hat{T_L}}{J}, \tag{6}$$

where n_p is the no. of pole pairs and J is of inertia of motor load system (kg m^2). The speed estimation methods in the adaptive rotor flux observer always desire some correction term in order to follow speed changes. This results in the estimation always lagging the actual values. In the natural observer, the speed estimation follows the speed changes simultaneously even for sudden change occurring in the load torque.

3. Modeling of two induction motors in parallel

Figure 3 shows the currents flow in the parallel connected induction motors fed by a single inverter. The inverter current is divided into two parts: i_{s1} and i_{s2}. If the current flow through the stator windings is equal, the circulating current will be zero and the parallel connected motors can be treated as a single motor. Current flow in each motor will not be equal if there is a difference in the wheel diameters or the motor parameters. In this situation, the average current and torque can be expressed as follows:

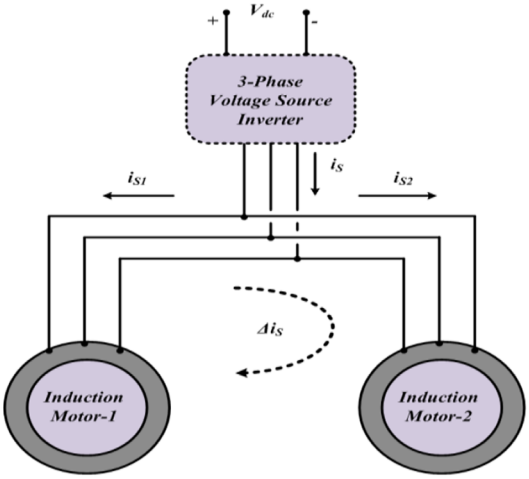

Figure 3. Current flow for parallel connected induction motor drives.

$$\hat{i}_s = \frac{i_{s1}+i_{s2}}{2} \bar{i}_s - \text{ Average of } i_{s1} \text{ and } i_{s2} \tag{7}$$

$$\bar{T}_e = \frac{T_1+T_2}{2} = T^*, \tag{8}$$

where T_1 and T_2 are derived from the speed controllers.

Average current $\bar{i}_s$ is compared with the reference current i_s^* to generate the control voltage for the inverter. Figure 4 shows the configuration of the parallel connected induction motor drive fed by a single inverter. The main components are speed estimator with adaptation algorithm, calculation block for reference currents, and current regulated pulse width modulated (CRPWM) voltage source inverter. With the measured line voltages and currents, the speeds of both motors are estimated and the torque reference of each motor is obtained from the speed error using PI controllers. The reference currents for average flux and average torque are derived by considering the average and differential parameters of the motors, stator currents, and rotor fluxes to make the system stable. Correspondingly, the space vector model of the induction motor is used to derive the reference current equations, which are as follows [1]:

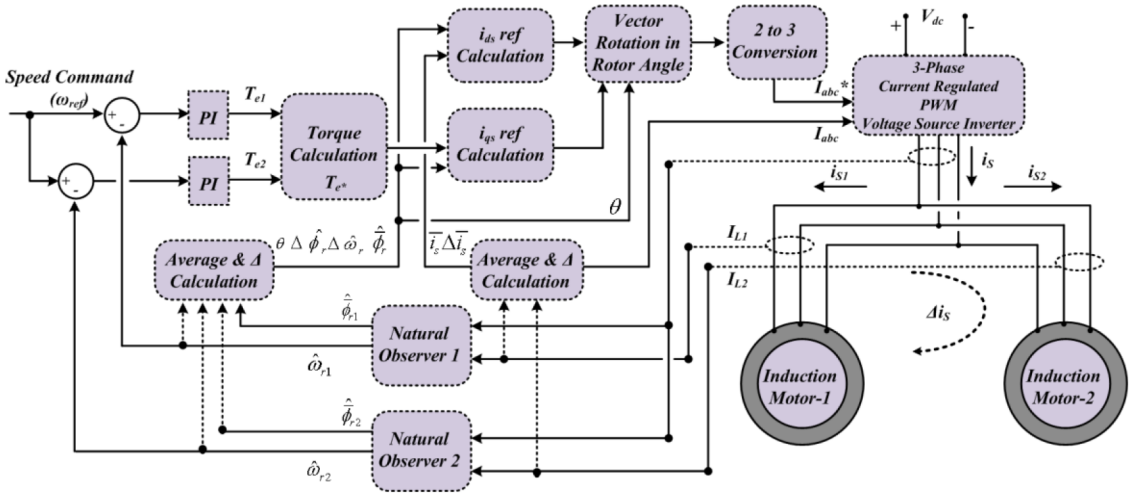

Figure 4. Configuration of parallel connected induction motor drives.

$$\bar{i_{ds}^{e*}}=\frac{\bar{S_r}\bar{\varphi_{dr}^{e*}}+\Delta\bar{\omega_r}\Delta\bar{\varphi_{qr}^{e}}+\Delta\bar{S_r}\Delta\bar{\varphi_{dr}^{e}}-\Delta\bar{U}\Delta\bar{i_{ds}^{e}}}{\bar{U}} \tag{9}$$

$$\bar{i_{qs}^{e*}}=\frac{\frac{\bar{T'}}{p\bar{M'}}-\Delta\bar{\hat{i}}_{ds}^{e}\times\Delta\bar{\hat{\varphi}}_{dr}^{e}+\Delta\bar{\hat{i}}_{qs}^{e}\times\Delta\bar{\hat{\varphi}}_{qr}^{e}}{\bar{\hat{\varphi}}_{dr}^{e*}} \tag{10}$$

$$\bar{T'}=\frac{\bar{T_e}-\left(\frac{\Delta\bar{M'}}{\bar{M'}}\right)\Delta\bar{T_e}}{1-\left(\frac{\Delta\bar{M'}}{\bar{M'}}\right)^2}, \tag{11}$$

where

$$U = S_r L_m \bar{U}=\frac{U_1+U_2}{2}\Delta\bar{U}=\frac{U_2-U_1}{2}$$

$$\bar{M'}=\frac{1}{2}\left(\frac{L_{m1}}{L_{r1}}+\frac{L_{m2}}{L_{r2}}\right)\Delta\bar{M'}=\frac{1}{2}\left(\frac{L_{m2}}{L_{r2}}-\frac{L_{m1}}{L_{r1}}\right)$$

$$\bar{i_s^e} = \frac{i_{s1}^e + i_{s2}^e}{2}\Delta\bar{i_s^e} = \frac{i_{s2}^e - i_{s1}^e}{2}$$

$$\bar{\hat{\omega}_r}=\frac{\hat{\omega}_{r1}+\hat{\omega}_{r2}}{2}\Delta\bar{\hat{\omega}}_r=\frac{\hat{\omega}_{r2}-\hat{\omega}_{r1}}{2}$$

$$\bar{S_r}=\frac{S_{r1}+S_{r2}}{2}\Delta\bar{S}_r=\frac{S_{r2}-S_{r1}}{2}$$

4. Simulation and experimental prototype results

Two identical three-phase squirrel cage induction motors of 745.6 W (1 HP) are used for parallel configuration. The Table shows the rating and parameters of the induction motor used for simulation and experimental setup. A direct field oriented sensorless vector control scheme is used to calculate the rotor angle from the estimated rotor fluxes. Simulations are carried out in MATLAB Simulink environment. The simulation blocks of sensorless vector control are constructed in MATLAB using power system blocksets and Simulink libraries. Induction motor and natural observer state equations are constructed in m-file and called back in Simulink model file. In addition, various simple blocks available in Simulink are used to construct the entire system. A PI controller is constructed using the PID block available in Simulink libraries. The experimental setup of the prototype model is shown in Figure 5. Hall effect current sensors and voltage sensors are used to measure the stator currents and voltages, respectively. The measured signals are processed in a TMS320F2812 DSP processor to estimate the speed, rotor fluxes, and stator currents. It also generates the PWM pulses to enable the IGBT switches. A three-phase IGBT based intelligent power module (IPM) performs the inverter operation. The simulation and experimental results are obtained for various running conditions.

4.1. Case (I) Balanced load condition

Both the induction motors run at a speed command of 900 rpm. At t = 2 s, a load of 2.5 Nm is applied to both motors. Figure 6 shows the simulation results for balanced load conditions. The estimated and actual speed waveforms are depicted in Figures 6(a) and 6(b) and it is inferred that both the motors follow the speed

command. There is a slight dip in the actual speed at the time of applying sudden load and it is negligible in the estimated speed. At steady state, the speed difference between the induction motors is zero. The estimated and actual load torque responses obtained by the simulation circuits are shown in Figures 6(c) and 6(d). The parameters of the torque controller are Kp = 0.08 and Ki = 0.2 and no limiter is placed in the torque estimator. At balanced load condition, the estimated speeds match the speed command and the estimated torque of both the motors follows the load torque. The d-q stator current waveforms for motor 1 and motor 2 are shown in Figure 6(e).

Table. Rating and parameters of induction motor.

Motor rating	
Output	745.6 W
Poles	4
Speed	1415 rpm
Frequency	50 Hz
Voltage	415 V
Current	1.8 A
R_s	19.355 Ω
R_r	8.43 Ω
L_s	0.715 H
L_r	0.715 H
L_m	0.689 H

Figure 5. Experimental setup of parallel connected induction motor drive controlled by DSP TMS320F2812.

The estimated speed waveform obtained by the experimental setup for a speed of 900 rpm and a load of 2.5 Nm is illustrated in Figure 7(a), which verifies that both the motors follow the speed command. The estimated torque waveform is shown in Figure 7(b). It follows the actual load torque, showing that the system is stable for balanced load conditions. The ripple in the estimated torque is much less for the applied inverter voltage and current. The d-q axes stator currents of motor 1 and motor 2 are depicted in Figures 7(c) and 7(d) and are identical.

4.2. Case (II) Unbalanced load condition

The unbalanced load condition arises whenever there is a slight dissimilarity in wheel diameter. To illustrate such conditions in simulation and experimental setup, unbalanced load is applied to both the motors. This is

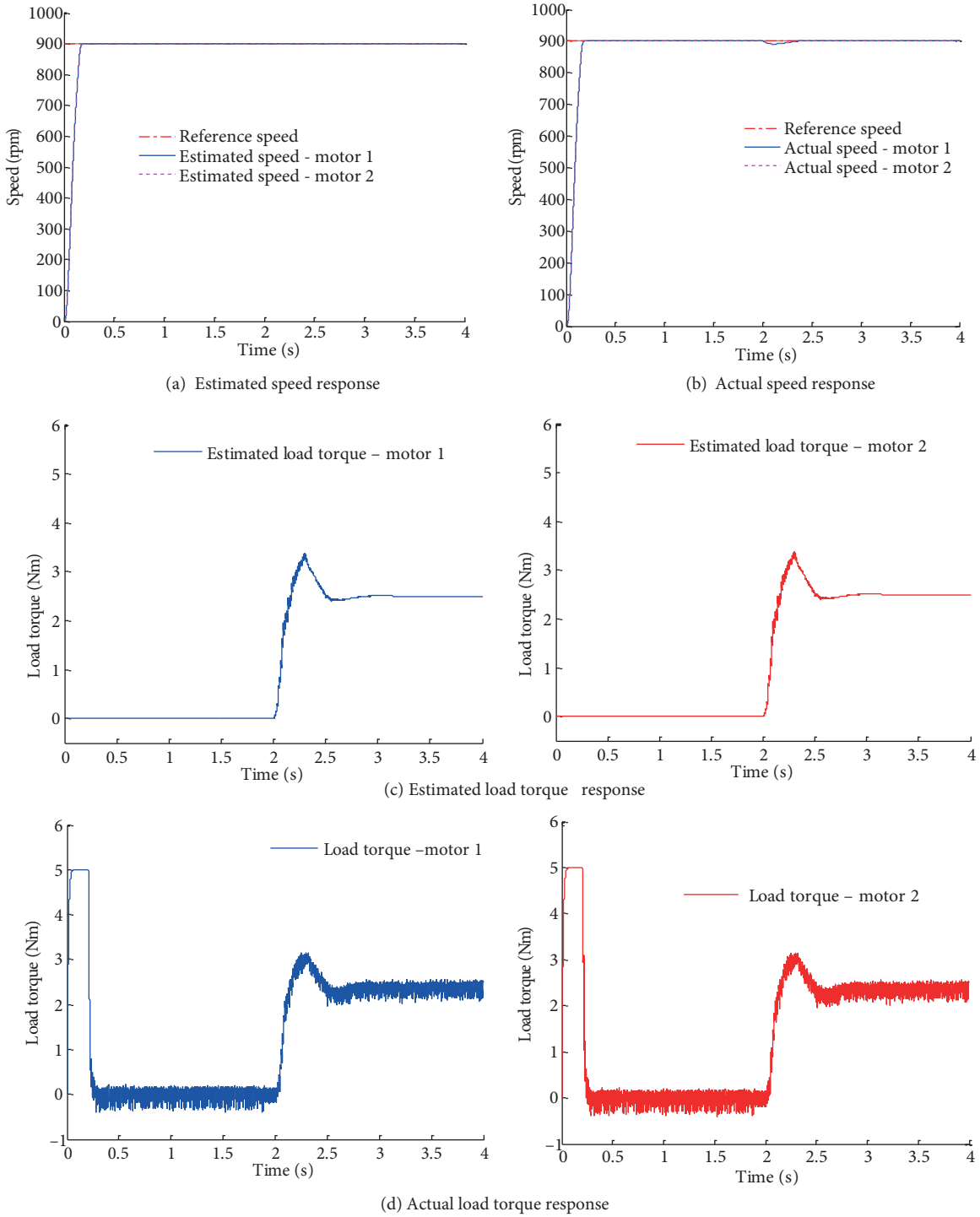

(a) Estimated speed response

(b) Actual speed response

(c) Estimated load torque response

(d) Actual load torque response

Figure 6. Simulation results for balanced load conditions.

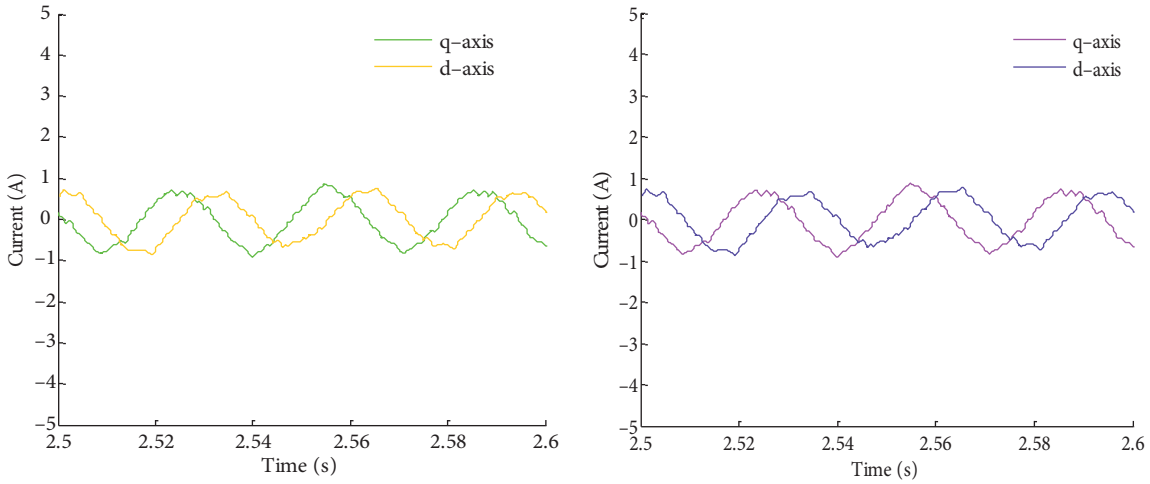

(e) Stationary reference frame stator current of motor 1 (green, yellow) and motor 2 (Pink, Purple)

Figure 6. Continued.

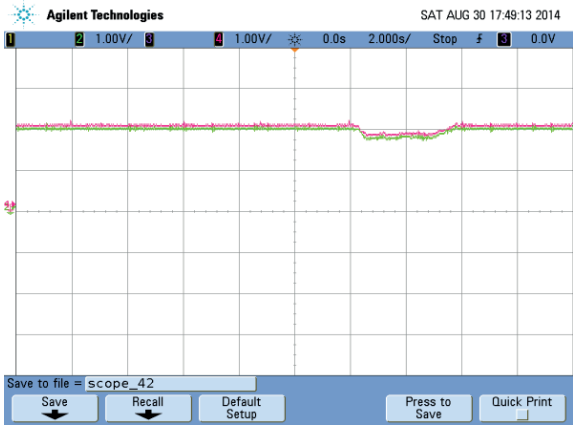

(a) Estimated speed response (500rpm/div)
(Green - Motor 1, Pink - Motor 2)

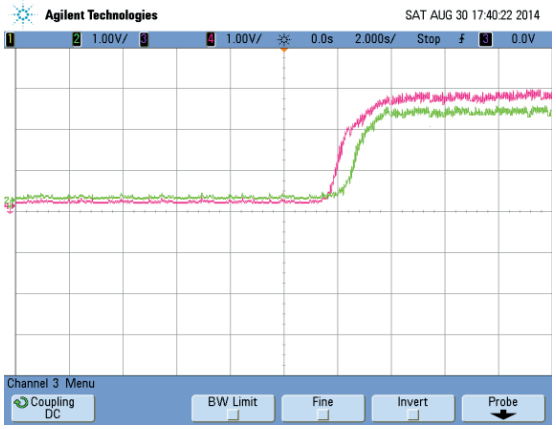

(b) Estimated load torque response (1Nm/div)
(Green - Motor 1, Pink - Motor 2)

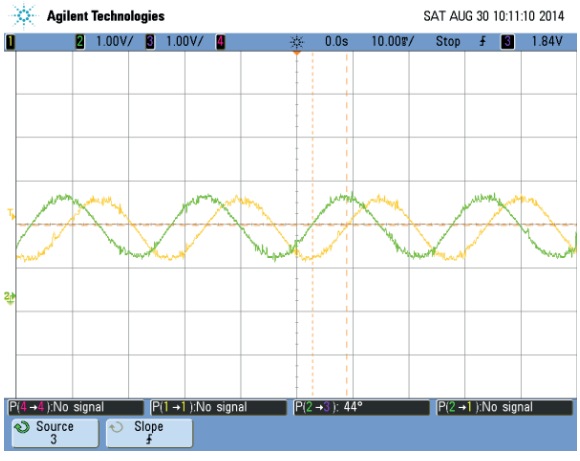

(c) Stationary reference frame stator
current current– motor 1(1A/div)

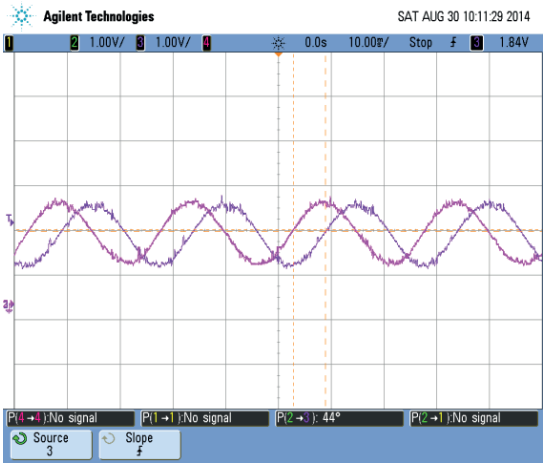

(d) Stationary reference frame stator
current current – motor 2 (1A/div)

Figure 7. Experimental results for balanced load conditions.

equivalent to slight dissimilarities in the wheel diameters. Both the induction motors run at a constant speed of 900 rpm. At t = 2 s, a load of 2.5 Nm is applied to motor 2 and motor 1 is at no load condition. This implies that the wheel diameter of motor 2 is larger than that of motor 1 and the torque of motor 2 is greater than that

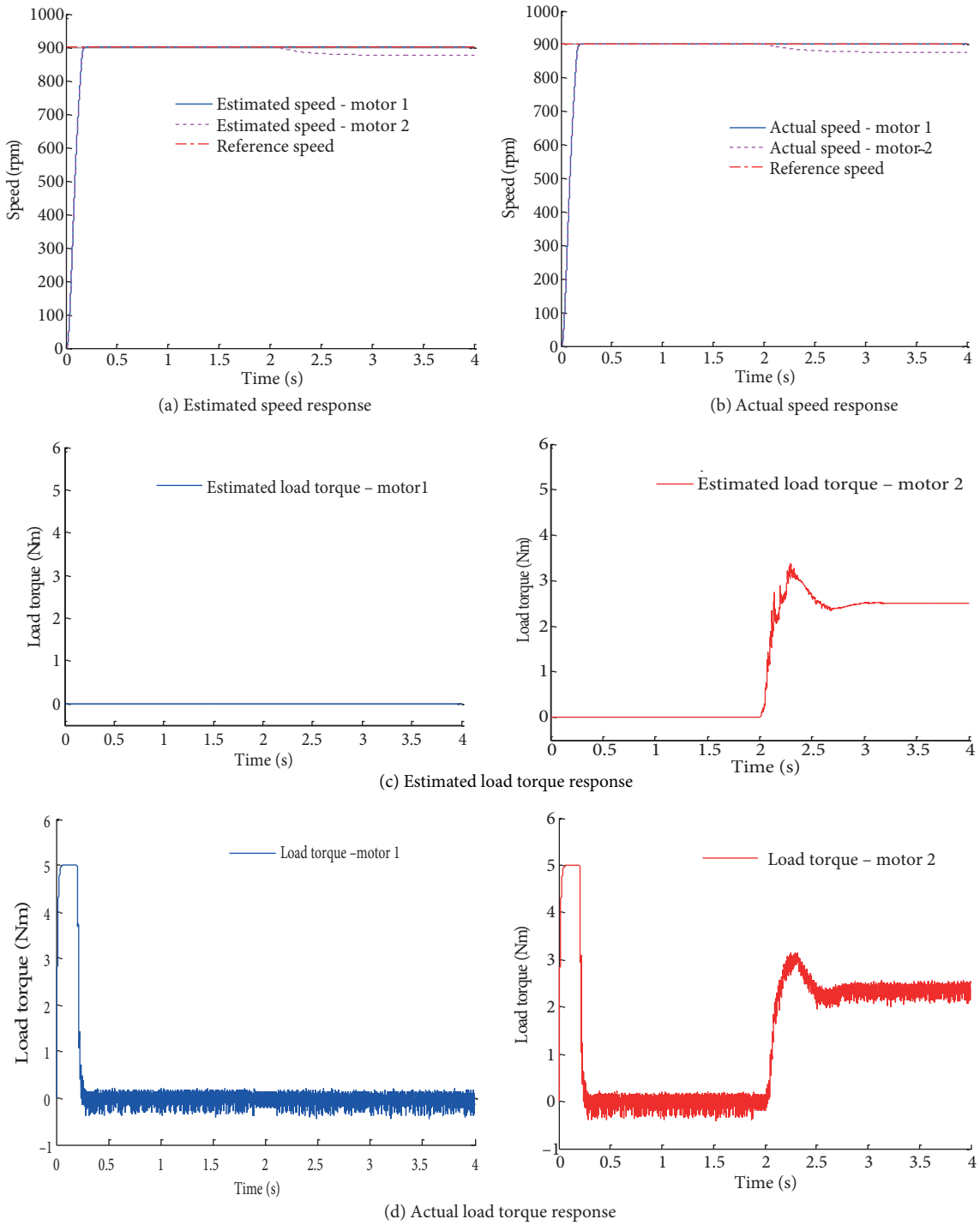

(a) Estimated speed response

(b) Actual speed response

(c) Estimated load torque response

(d) Actual load torque response

Figure 8. Simulation results for unbalanced load conditions.

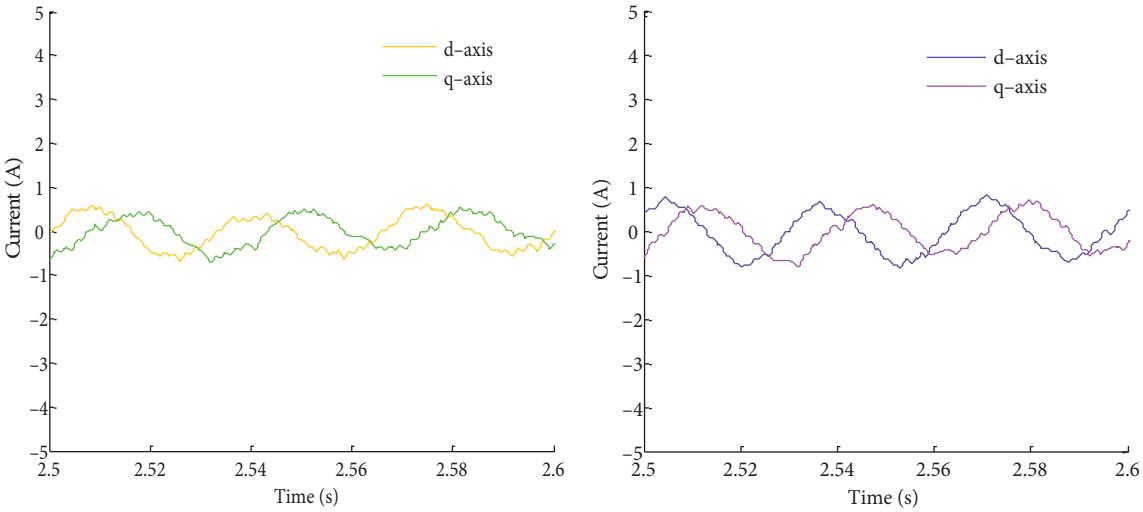

(e) Stationary reference frame stator current current – motor 1(green, yellow) and motor 2 (pink, purple)

Figure 8. Continued.

of motor 1. Figure 8 shows the simulation results for unbalanced load conditions. The estimated and actual speeds of both the motors are given in Figures 8(a) and 8(b). In the simulation waveform, the speed of motor 2 decreases to 880 rpm and the speed of motor 1 remains the same. The speed difference between the motors under steady state is 20 rpm. With respect to the reference speed, the speed of motor 2 deviates by 20 rpm (2.22%). The speed of the motor 2, which is loaded, is not equal to the command speed under unbalanced load conditions. However, both the motors run at steady speed. This makes the system stable under unbalanced load conditions. The estimated and actual torque responses of both the motors are shown in Figures 8(c) and 8(d) respectively, while Figure 8(e) illustrates the dq - axes stator current waveforms of motor 1 and motor 2.

The performance of the natural observer is compared with the conventional adaptive observer method for unbalanced load conditions. Figured 9(a) and 9(b) show the estimated and actual speed responses of motor

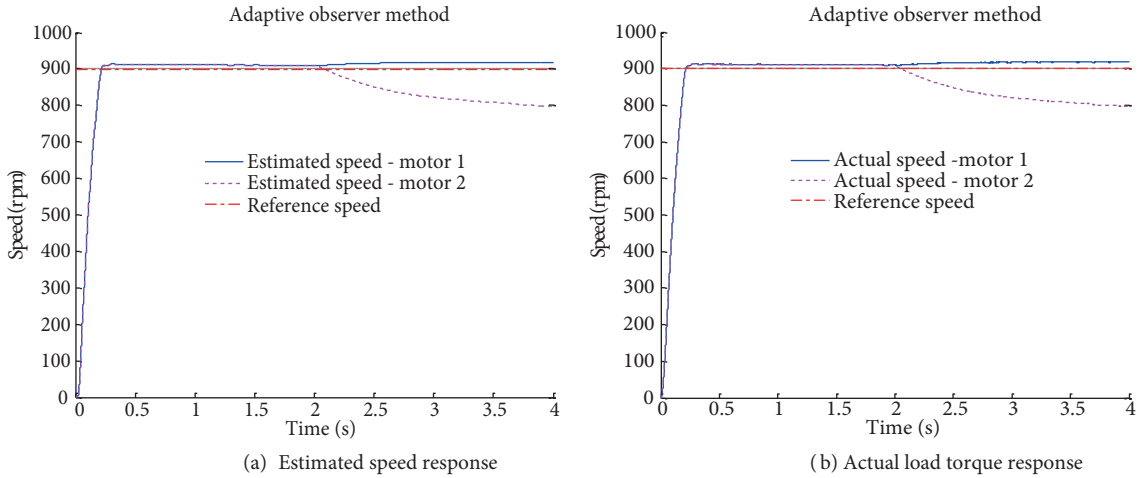

(a) Estimated speed response

(b) Actual load torque response

Figure 9. Simulation results of conventional adaptive observer for unbalanced load conditions.

1 and motor 2 for unbalanced load conditions. In the adaptive observer method, the estimated speed of motor 2 decreases to 800 rpm and the speed of motor 1 increases to 920 rpm. The speed difference between the motors under steady state is 120 (13.33%) rpm. The speed difference between motor 1 and speed command is 20 rpm (2.22%) and the speed difference between motor 2 and speed command is 100 rpm (11.11%). In the natural observer method, the speed difference of the motors under steady state is 20 (2.22%) rpm. The speed difference among the induction motors for unbalanced load conditions is less in the natural observer.

The estimated speed response obtained by the experimental setup when load is applied to motor 2 is shown in Figure 10(a). It is known that the estimated speed follows the speed command and speed deviation is observed under unbalanced load conditions. The estimated torque responses of motor 1 and motor 2 are shown in Figure 10(b) and the dq - axes stator current waveforms for motor 1 and motor 2 are shown in Figures 10(c) and 10(d), respectively.

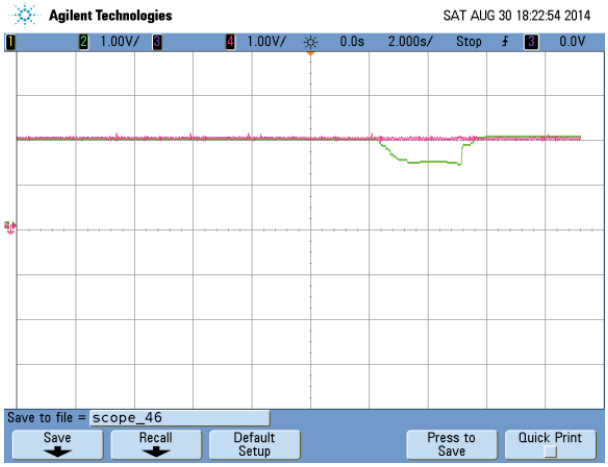

(a) Estimated speed response motor - 2 loaded (500 rpm/div) (green - motor 1, purple - motor 2)

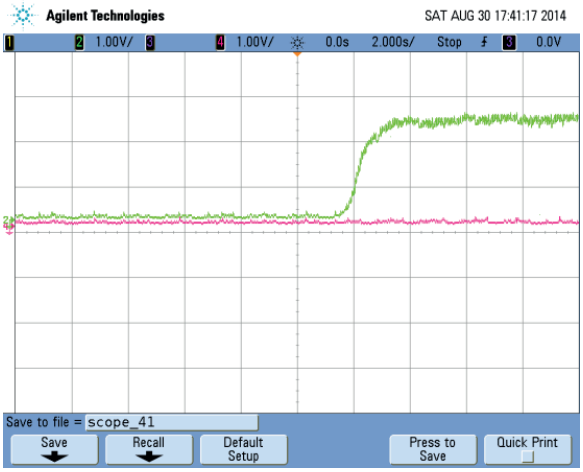

(b) Estimated load torque response motor - 2 loaded (1Nm/div) (green - motor 1, purple - motor 2)

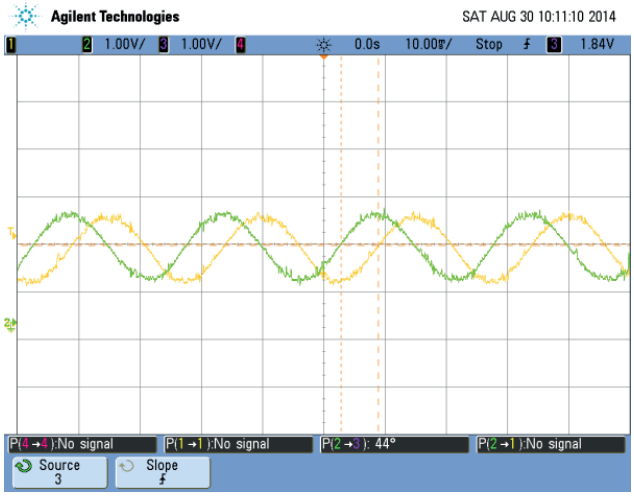

(c) Stationary reference frame stator current – motor 1(1A/div)

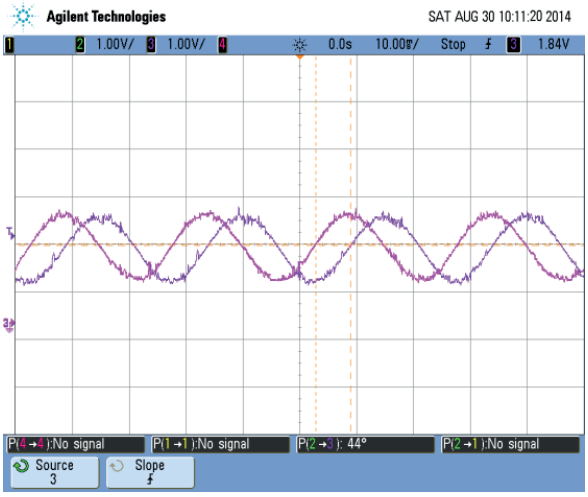

(d) Stationary reference frame stator current – motor 2 (1A/div)

Figure 10. Experimental results for unbalanced load conditions – motor 2 is loaded.

4.3. Case (III) Step change in speed with constant load

Both the motors run at a constant load of 2.5 Nm with a speed of 900 rpm initially. To prove the performance of the drive for constant load with step change in speed operation, the reference speed of the motors is decreased from 900 rpm to 600 rpm at t = 1 s. Figure 11 shows the simulation results of motor 1 and motor 2 for constant load with variable speed conditions. Figures 11(a) and 11(b) show the performance of motor 1 and motor 2, respectively. At t = 2 s, the speed command is increased from 600 rpm to 900 rpm. It is observed that the actual and estimated speeds of both the induction motors follow the speed command quickly and the steady state error is zero. The simulation results confirm that for a step change in speed with constant load conditions the speed and torque of the parallel connected two motors follow the set conditions with smooth propagation of torque and speed.

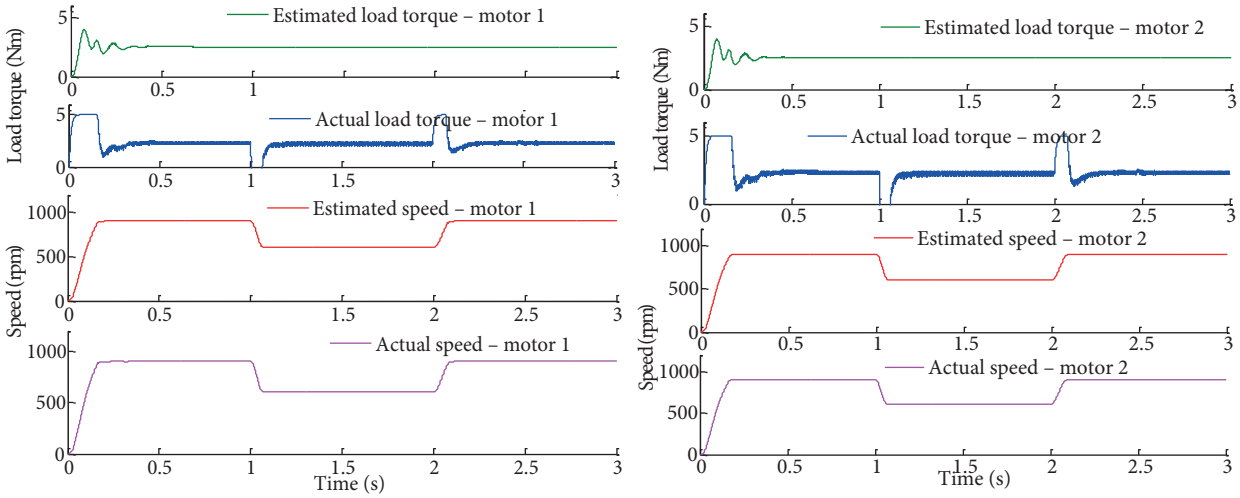

(a) Response of motor 1 (b) Response of motor 2

Figure 11. Simulation results for step change in speed with constant load.

5. Conclusions

In this paper, a natural observer with load torque adaption is employed to estimate the speeds of parallel connected induction motors fed by a single inverter. The induction motor and natural observer are modeled in MATLAB with a state space model and simulations are carried out for different running conditions. It is concluded that the estimated parameters such as rotor speed and load torque follow the command value and the error is zero at steady state. The ripple is much less in the estimated torque for the applied inverter voltage and current. The convergence rates are also fast. Hardware results are presented to validate the performance of the natural observer and they match with the simulation results. The speed deviations for unbalanced load conditions are reduced in this proposed method compared with the conventional adaptive observer method.

Nomenclature

A	State matrix	$\bar{\omega}_r$	Average rotor speed of motor 1 and motor 2 respectively (rad/s)
X	State vector	$\bar{\Delta\omega}_r$	Difference average rotor speed of motor 1 and motor 2 respectively (rad/s)
B	Input matrix	$i^s_{ds} i^s_{qs}$	d-axis and q-axis stator current in stator reference frame (A)
V_s	Input vector	$\hat{i}^s_{ds} \hat{i}^s_{qs}$	Estimated d-axis and q-axis stator current in stator reference frame (A)
C	Output matrix	$i^e_{ds} i^e_{qs}$	d-axis and q-axis stator current in synchronous reference frame (A)
Y	Output vector	$\hat{i}^e_{ds} \hat{i}^e_{qs}$	Estimated d-axis and q-axis stator current in synchronous reference frame (A)
R_s	Stator resistance (Ω)	$\hat{\Delta i}^e_{ds} \Delta \hat{i}^e_{qs}$	Estimated difference in d-axis and q-axis stator current of motor 1 and motor 2 in synchronous reference frame (A)
R_r	Rotor resistance (Ω)	$i_{s1} i_{s2}$	Stator current of motor 1 and 2 respectively (A)
L_s	Stator self-inductance (H)	$\bar{i}_s$	Average stator current of motor 1 and 2 (A)
L_{s1}, L_{s2}	Stator self-inductance of motor 1 and motor 2 respectively (H)	$\hat{\bar{i}}_s$	Estimated average stator current of motor 1 and 2 (A)
L_r	Rotor self-inductance (H)	i^*_s	Reference stator current (A)
L_{r1}, L_{r2}	Rotor self-inductance of motor 1 and motor 2 respectively (H)	$V^s_{ds} V^s_{qs}$	d-axis and q-axis stator voltage in stator reference frame (V)
L_m	Mutual inductance (H)	$V^e_{ds} V^e_{qs}$	d-axis and q-axis stator voltage in synchronous reference frame (V)
L_{m1}, L_{m2}	Mutual inductance of motor 1 and motor 2 respectively (H)	$\varphi^s_{dr} \varphi^s_{qr}$	d-axis and q-axis rotor flux in stator reference frame (Wb)
σ	Leakage coefficient	$\hat{\varphi}^s_{dr} \hat{\varphi}^s_{qr}$	Estimated d-axis and q-axis rotor flux in stator reference frame (Wb)
τ_r	Rotor time constant	$\varphi^e_{dr} \varphi^e_{qr}$	d-axis and q-axis rotor flux in synchronous reference frame (Wb)
n_p	No. of pole pairs	$\varphi^e_{r1} \varphi^e_{r2}$	Rotor flux of motor 1 and motor 2 in synchronous reference frame respectively (Wb)
J	Inertia of the motor load system (kg m^2)	$\hat{\varphi}^e_{dr} \hat{\varphi}^e_{qr}$	Estimated d-axis and q-axis rotor flux in synchronous reference frame (Wb)
P	Differential operator	$\hat{\Delta\varphi}^e_{r1}$	Estimated difference in rotor flux of motor 1 and motor 2 in synchronous reference frame respectively (Wb)
'^'	Represents estimated values	$\Delta\hat{\varphi}^e_{r2}$	
K_D	Differential gain	$\bar{\varphi}^e_r$	Average rotor flux of motor 1 and motor 2 respectively (Wb)
K_P	Proportional gain	$\bar{\Delta\varphi}^e_r$	Difference average rotor flux of motor 1 and motor 2 respectively (Wb)
K_I	Integral gain	T_L	Load torque (Nm)
ω_r	Rotor angular velocity (rad/s)	$\hat{T}_L$	Estimated load torque (Nm)
$\hat{\omega}_r$	Estimated rotor angular velocity (rad/s)	T_e	Electromagnetic torque developed (Nm)
ω_e	Synchronous rotor angular velocity (rad/s)	T_1, T_2	Load torque of motor 1 and motor 2 respectively (Nm)
ω_{r1}, ω_{r2}	Rotor angular velocity of motor 1 and motor 2 respectively (rad/s)	$\bar{T}_e$	Average load torque of motor 1 and motor 2 (Nm)

References

[1] Matsuse K, Kouno Y, Kawai H, Oikawa J. Characteristics of speed sensorless vector controlled dual induction motor drive connected in parallel fed by a single inverter. IEEE T Ind Appl 2004; 40: 153-161.

[2] Azegami K, Takahashi Y, Matsuse K, Ito S, Nakajima Y. Speed characteristics of sensorless vector controlled two unbalanced induction motor drive fed by single inverter. In: IEEE 2012 Electrical Machines and Systems Conference; 21–24 October 2012; Sapporo, Japan: IEEE. pp. 1-5.

[3] Kawai H, Kouno Y, Matsuse K. Characteristics of speed sensorless vector control of parallel connected dual induction motor fed by a single inverter. In: IEEE 2002 Power Conversion Conference; 02–05 April 2002; Osaka, Japan: IEEE. pp. 522-527.

[4] Matsuse K, Kouno Y, Kawai H, Yokomizo S. A speed sensorless vector control method of parallel connected dual induction motor fed by a single inverter. IEEE T Ind Appl 2002; 38: 1566-1571.

[5] Osawa A, Yamazaki M, Matsuse K. Vector control method of parallel connected induction motor drives fed by a matrix converter. In: IEEE 2011 Industry Applications Society Annual Meeting; 9–13 October 2011; Orlando, Florida, FL, USA: IEEE. pp. 1-7.

[6] Yamazaki M, Sakaki K, Matsuse K. Characteristics of vector control of two induction motor drives fed by matrix converter. In: IEEE 2012 Electrical Machines and Systems Conference; 21–24 October 2012; Sapporo, Japan: IEEE. pp. 1-5.

[7] Xu F, Shi L. Unbalanced thrust control of multiple induction motors for traction system. In: IEEE 2011 Industrial Electronics and Applications Conference; 21–23 June 2011; Beijing, China: IEEE. pp. 2752-2757.

[8] Lee HW. Study on motor characteristics due to deviation of the wheel diameters with parallel operation. J Electr Eng Technol 2013; 8: 106-109.

[9] Xu F, Shi L, Li Y. The weighted vector control of speed-irrelevant dual induction motors fed by the single inverter. IEEE T Power Electron 2013; 28: 5665-5672.

[10] Matsumoto Y, Osawa C, Mizukami T, Ozaki S. A stator flux based vector control method for parallel connected multiple induction motors fed by a single inverter, In: IEEE 1998 Applied Power Electronics Conference and Exposition; 15–19 February 1998; Anaheim, CA, USA; IEEE. pp. 575-580.

[11] Taniguchi M, Yoshinaga T, Matsuse K. A speed-sensorless vector control of parallel connected multiple induction motor drives with adaptive rotor flux observers. In: IEEE 2006 Power Electronics Specialists Conference; 18–22 June 2006; Jeju, Korea: IEEE. pp. 1-5.

[12] Inoue T, Azegami K, Matsuse K, Ito S, Nakajima Y. Dynamic performance of sensorless vector controlled multiple induction motor drive connected in parallel fed by single inverter. In: IEEE 2011 Industry Applications Society Annual Meeting; 9–13 October 2011; Orlando, Florida, FL, USA: IEEE. pp. 1-6.

[13] Kouno Y, Kawai H, Yokomizo S, Matsuse K. A speed sensorless vector control method of parallel connected dual induction motor fed by a single inverter. In: IEEE 2001 Industry Applications Conference; 30 September–04 October 2001; Chicago, Illinois, IL, USA: IEEE. pp. 1218-1223.

[14] Kelecy PM, Lorenz RD. Control methodology for single inverter parallel connected dual induction motor drives for electric vehicles. In: IEEE 1994 Power Electronics Specialists Conference; 20–25 June 1994; Taipei, Taiwan: IEEE. pp. 987-991.

[15] Bowes SR, Sevinc A, Holliday D. New natural observer applied to speed sensorless dc servo and induction motors. IEEE T Ind Appl 2004; 51: 1025-1032.

[16] Gunabalan R, Subbiah V. Speed sensorless vector control of parallel connected induction motor drive with fuzzy controller. In: IEEE 2012 Computational Intelligence and Computing Research Conference; 18–20 December 2012; Coimbatore, TamilNadu, India: IEEE. pp. 473-478.

[17] Febin Daya L, Subbiah V, Sanjeevikumar P. Robust speed control of an induction motor drive using wavelet-fuzzy based self-tuning multi-resolution controller. Int J Comput Int Sys 2013; 6: 724-738.